LAWRENCE
LIVERMORE
NATIONAL
LABORATORY

UCRL-JRNL-229734

Absolute and Relative Surrogate Measurements of the 236U(n,f) Cross Section as a Probe for Angular Momentum Effects

B.F. Lyles, L.A. Bernstein, J.T. Burke, J. Escher, I. Thompson, F.S. Dietrich, L. Phair, D.L. Bleuel, J. Gibelin, M. Wiedeking, M.A. McMahan, E. Rodroguez-Vieitez, R.M. Clark, A.O. Macchiavelli, S.R. Lesher, B. Darakchieva, M. Evtimova, C.W. Beausang, P. Fallon

April 5, 2007

Physical Review C

Absolute and Relative Surrogate Measurements of the ^{236}U(n,f) Cross Section as a Probe for Angular Momentum Effects

B.F. Lyles,* L.A. Bernstein, J.T. Burke, F.S. Dietrich, J. Escher, and I. Thompson
Lawrence Livermore National Laboratory, Livermore, California, 94551

D.L. Bleuel, R.M. Clark, P. Fallon, J. Gibelin, A.O. Macchiavelli,
M.A. McMahan, L. Phair, E. Rodriguez-Vieitez, and M. Wiedeking
Lawrence Berkeley National Laboratory, Berkeley, California, 94720

C.W. Beausang, S.R. Lesher, B. Darakchieva, and M. Evtimova
Department of Physics, University of Richmond, Richmond, Virginia, 23173
(Dated: April 3, 2007)

Using both the absolute and relative surrogate techniques, the ^{236}U(n,f) cross section was deduced over an equivalent neutron energy range of 0 to 20 MeV. A 42 MeV ^{3}He beam from the 88–Inch Cyclotron at Lawrence Berkeley National Laboratory was used to perform a (^{3}He,α) pickup reaction on targets of ^{235}U ($J^{\pi}=7/2^{-}$) and ^{238}U ($J^{\pi}=0^{+}$) and the fission decay probabilities were determined. The ^{235}U(^{3}He,αf) and ^{238}U(^{3}He,αf) were surrogates for ^{233}U(n,f) and ^{236}U(n,f), respectively. The cross sections extracted using the Surrogate Method were compared to directly measured cross sections. The sensitivity of these cross sections to the J^{π}-population distributions was explored.

PACS numbers: 24.10.-i, 24.75.+i, 25.55.-e, 25.85.Ge

I. INTRODUCTION

Due to the high radioactivity and short lifetimes of many nuclear species of interest, the direct determination of neutron-induced reaction cross sections in the laboratory is difficult. Surrogate reaction techniques [1, 2] obviate this issue by measuring the relevant decay probability of the desired compound nucleus, produced by an alternative reaction, using a stable target and beam. The external Surrogate Ratio Method (SRM) [3] is a variation on the absolute surrogate technique in which the *same* exit channel probability for two *different* compound nuclei is measured and the unknown cross section of interest is extracted relative to a known cross section. The SRM has the advantage that it removes the need to measure the total number of reaction events, thus eliminating what was formerly the largest source of systematic uncertainty in surrogate measurements.

Early absolute surrogate measurements showed discrepancies from directly measured neutron-induced fission cross sections, with errors on the order of 15–20% at low energies [2]. By properly modeling the angular momentum dependence of fission probabilities, semi-empirical work by Younes and Britt demonstrated more accurate deduced cross sections [4]. This suggested a mismatch of spin in the entrance channel, where different angular momentum population distributions arise from the neutron-induced reaction as compared to the surrogate reaction. This suggestion is supported by the recent theoretical work of Thompson and Escher [5] in which spin distributions generated using a (^{3}He,α) pickup reaction on ^{238}U and ^{235}U were found to be markedly different from the spin distributions induced in the same compound nucleus generated from a neutron-induced reaction [6]. The SRM has been shown to reduce the effect of spin mismatch in the entrance channel when inferring neutron-induced fission cross sections [7]. In recent SRM experiments [8–10], neutron-induced fission cross sections were extracted with systematic uncertainties of 5–10% in range from 0 to 20 MeV. Even-even targets were used in an attempt to mimic the spin distribution generated by the neutron-induced entrance channel via a surrogate (α, α') entrance channel.

To test the limits of the surrogate technique, surrogate measurements using a (^{3}He,α) entrance channel were performed on targets with different ground-state spins and parities, ^{238}U ($J^{\pi}=0^{+}$) and ^{235}U ($J^{\pi}=7/2^{-}$). In Section II, the theoretical framework for absolute surrogate and surrogate ratio techniques is outlined and a description of the effects of angular momentum and parity distributions on the experimental observables is established. Section III consists of a description of the experimental layout and electronics configuration. In Section IV, the ^{236}U(n,f) cross sections obtained using the absolute surrogate technique and SRM are discussed. In both cases, the ^{236}U(n,f) cross section was deduced over an equivalent neutron energy range of 0 to 20 MeV. The SRM made use of the relatively well-measured ^{233}U(n,f) cross section. These were compared to directly measured cross sections and the effect of angular momentum mismatch on the extracted cross sections was investigated. Concluding remarks are given in Section V.

*Also at Department of Nuclear Engineering, University of California, Berkeley, Berkeley California 94720.; Electronic address: bethany@nuc.berkeley.edu

II. THEORY

The Hauser-Feshbach cross section formulation [11] assumes compound nucleus formation and is given by the following expression:

$$\sigma_{\alpha\chi} = \sum_{J,\pi} \sigma_{\alpha}^{CN}(E^*, J, \pi) G_{\chi}^{CN}(E^*, J, \pi) \quad (1)$$

where α is the desired reaction entrance channel (in this case, n + ^{233}U or n + ^{236}U), E* is the excitation energy of the compound nucleus, related to the energy of the neutron in the center of mass, E$_{cm}$, by $E^* = E_{cm}$ + S$_n$, where S$_n$ is the neutron separation energy, and χ is the exit channel (here, the fission decay mode). Cross sections are usually given as a function of the projectile energy, while decay probabilities are typically given as a function of the excitation energy of the decaying nucleus. In the present paper, we will denote all quantities as a function of excitation energy, with the exception of the final, deduced cross sections. The reaction cross section, $\sigma_{\alpha\chi}$, is given by the summation over all total angular momentum, J, and parity, π, states of the formation cross sections, $\sigma_{\alpha}^{CN}(E^*, J, \pi)$, multiplied by the decay probabilities, $G_{\chi}^{CN}(E^*, J, \pi)$, as a function of excitation energy, spin and parity in the compound system. An analogous expression can be written for the surrogate reaction, which gives the probability for forming the same composite nucleus via the surrogate entrance channel δ and its subsequent decay via fission:

$$P_{\delta\chi}(E^*) = \sum_{J,\pi} F_{\delta}^{CN}(E^*, J, \pi) G_{\chi}^{CN}(E^*, J, \pi) \quad (2)$$

Here F$_{\delta}^{CN}(E^*, J, \pi)$ are the direct-reaction probabilities, in this case the probabilities for (^{3}He,α) pickup on various states in ^{235}U or ^{238}U.

To directly compare the decay probabilities resulting from the desired and surrogate reactions, consider the following equivalent expression for Equation 1.

$$\sigma_{\alpha\chi}(E^*) = \sigma_{\alpha}^{form}(E^*) P_{\alpha\chi}(E^*) \quad (3)$$

where

$$P_{\alpha\chi}(E^*) = \sum_{J,\pi} F_{\alpha}^{CN}(E^*, J, \pi) G_{\chi}^{CN}(E^*, J, \pi) \quad (4)$$

Here, $\sigma_{\alpha}^{form}(E^*)$ is the cross section for forming the compound nucleus via the desired reaction and $F_{\alpha}^{CN}(E^*, J, \pi)$ are the desired reaction probabilities. The corresponding equation for the surrogate reaction entrance channel is

$$\sigma_{\delta\chi}(E^*) = \sigma_{\delta}^{form}(E^*) \sum_{J,\pi} F_{\delta}^{CN}(E^*, J, \pi) G_{\chi}^{CN}(E^*, J, \pi) \quad (5)$$

where $\sigma_{\delta}^{form}(E^*)$ is the cross section for forming the compound nucleus via the surrogate reaction and the sum is the experimentally determined surrogate reaction fission probability from Equation 2.

In the Weisskopf-Ewing limit of the Hauser-Feshbach theory [12], the probability for decay into a given exit channel χ, or branching ratio G_{χ}, is independent of the total angular momentum and parity of the populated state. $P_{\delta\chi}$ from Equation 2 and $P_{\alpha\chi}$ from Equation 4 should be equal if

1. the Weisskopf-Ewing approximation applies for the range of populated J$^{\pi}$ states and energies considered

   or

2. $F_{\alpha}^{CN}(E^*, J, \pi) \approx F_{\delta}^{CN}(E^*, J, \pi)$ for the energies considered.

Assuming that ENDF/B-VII [13] gives an accurate neutron-induced fission cross section for Equation 3 and that an accurate calculation of $\sigma_{\alpha}^{form}(E^*)$ is feasible, discrepancies in the cross sections obtained from an absolute surrogate experiment imply an angular momentum mismatch in the composite nuclei generated from the two entrance channels, inapplicability of the Weisskopf-Ewing approximation, or both.

If the Weisskopf-Ewing approximation holds, the branching ratios, G_{χ}, can be taken out of the summation over all total angular momentum and parity states in Equations 1 and 2. The formula for the desired reaction cross section simplifies to

$$\sigma_{\alpha\chi}(E^*) = \sigma_{\alpha}^{CN}(E^*) G_{\chi}^{CN}(E^*) \quad (6)$$

and for the surrogate reaction,

$$P_{\delta\chi}(E^*) = G_{\chi}^{CN}(E^*) \quad (7)$$

These results are combined and the expression for the desired reaction cross section in terms of the surrogate reaction decay probability is given by

$$\sigma_{\alpha\chi}(E^*) = \sigma_{\alpha}^{CN}(E^*) P_{\delta\chi}(E^*) \quad (8)$$

For an absolute surrogate measurement, the neutron-induced formation cross sections, $\sigma_{\alpha}^{CN}(E^*)$, can be determined via an optical model calculation with uncertainties on the order of 5% [14]. The surrogate reaction fission probabilities

$$P_{\delta\chi}(E^*) = \frac{N_{\delta f}(E^*)}{N_{\delta}(E^*)} \quad (9)$$

are measured experimentally, where $N_{\delta f}$ is the number of alpha particles in coincidence with fission and N_{δ} is the total number of direct-reaction events. The results of such an analysis are discussed in Sections IV A and IV B.

For neutron-induced reactions on actinides, the desired reaction cross sections involving two different nuclei, but the same exit channel can also be measured relative to

one another, as described below in the Weisskopf-Ewing limit.

$$R = \frac{\sigma_{\alpha_1\chi}}{\sigma_{\alpha_2\chi}} = \frac{\sigma^{CN}_{\alpha_1} P_{\delta_1\chi}}{\sigma^{CN}_{\alpha_2} P_{\delta_2\chi}} \tag{10}$$

The ratio of surrogate reaction probabilities is given by

$$\frac{P_{\delta_1\chi}(E^*)}{P_{\delta_2\chi}(E^*)} = \frac{N_{\delta_1 f}(E^*)}{N_{\delta_1}(E^*)} \frac{N_{\delta_2}(E^*)}{N_{\delta_2 f}(E^*)} \tag{11}$$

The total number of reaction events is highly sensitive to target contamination and was formerly the largest source of systematic uncertainty in surrogate measurements. However, the experiment is tailored such that the total numbers of reaction events are equal within a normalization factor,

$$N_{\delta_2} = A_{norm} N_{\delta_1} \tag{12}$$

where A_{norm} is dependent upon the total number of atoms in the target, integrated beam intensity and live time of the data acquisition. Thus, the ratio is independent of the total number of reaction events and becomes

$$R(E^*) = \frac{\sigma^{CN}_{\alpha_1}(E^*) N_{\delta_1 f}(E^*) A_{norm}}{\sigma^{CN}_{\alpha_2}(E^*) N_{\delta_2 f}(E^*)} \tag{13}$$

In the SRM, the formation cross sections for the two reactions are assumed to be sufficiently similar, a reasonable assumption given that the optical model observables vary slowly over the range of uranium isotopes considered, and the expression for the ratio is reduced to

$$R(E^*) = \frac{N_{\delta_1 f}(E^*) A_{norm}}{N_{\delta_2 f}(E^*)} \tag{14}$$

The unknown cross section is obtained by multiplying the ratio by the known neutron-induced reaction cross section matched at excitation energy and then shifting the result into equivalent neutron energy. Equivalent neutron energy, E_n, is defined as the energy of the neutron in the desired reaction and is related to the excitation energy of the compound nucleus, E^*, by $E_n = E^* - S_n$, where S_n is the separation energy of the neutron in the compound system. The results of such a ratio analysis are discussed in Section IV C.

In analogy to the case for the absolute surrogate analysis, the ratio of the neutron-induced fission cross sections should be equal to the ratio of the surrogate fission cross sections if

1. $\sigma^{form}_{\alpha_1} = \sigma^{form}_{\alpha_2}$ over the energy range considered **and** the Weisskopf-Ewing approximation holds for both CN involved in the ratio

   or

2. $\sigma^{form}_{\alpha_1} = \sigma^{form}_{\alpha_2}$ over the energy range considered **and** $F^{CN}_{\alpha_1}(E^*, J, \pi) \approx F^{CN}_{\delta_1}(E^*, J, \pi)$ and $F^{CN}_{\alpha_2}(E^*, J, \pi) \approx F^{CN}_{\delta_2}(E^*, J, \pi)$ for the energies considered.

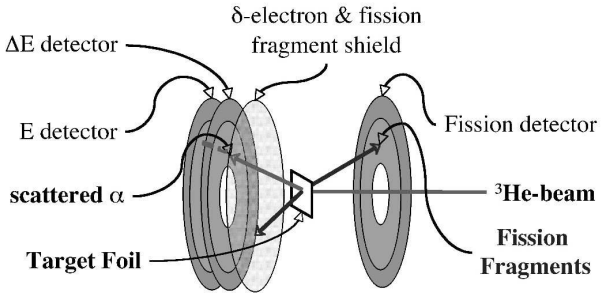

FIG. 1: Schematic of STARS Experimental Setup

The Surrogate Method, as applied in the past in almost all situations, assumes that the Weisskopf-Ewing limit of the statistical Hauser-Feshbach theory applies. However, in the experiments described below, at low excitation energies in the compound nucleus and in the energy regimes corresponding to the onset of first and second chance fission, where fission tends to proceed through discrete transition states, we expect the Weisskopf-Ewing approximation to break down and the branching ratios to be J^π-dependent. Such a breakdown should manifest itself as discrepancies between the cross sections extracted using the Surrogate Method and directly measured neutron-induced cross sections.

III. EXPERIMENTAL APPARATUS

A 42 MeV $^3He^{2+}$ beam from the 88–Inch Cyclotron at Lawrence Berkeley National Laboratory was employed in the experiment. Data were taken over a period of 8 days with beam intensity fluctuating between 2 and 3 enA. The ^{238}U target was a self-supporting metallic foil with a thickness of 4709 ± 235 angstroms (761 ± 38 μg/cm^2). The ^{235}U target was prepared as the nitrate salt of approximately 720 μg/cm^2 thickness, stippled on a 100 μg/cm^2 natural carbon backing. The isotopic composition of the target was 99.34% ^{235}U, 0.04% ^{234}U and 0.62% ^{238}U. The reaction products were detected using the Silicon Telescope Array for Reaction Studies (STARS), as shown in Figure 1. STARS was comprised of a particle telescope consisting of two double-sided Micron Semiconductor S2 type silicon detectors (22 mm active inner diameter and 70 mm active outer diameter), a 140 μm ΔE detector and a 1002 μm E detector, covering a forward angle range of 36° to 66° relative to the beam axis. The targets were located 15 mm upstream from the front face of the ΔE detector. The ΔE and E detectors were spaced 3 mm apart. The beam spot on the target was approximately 3 mm in diameter. A 4.44 mg/cm^2 aluminum foil, biased to 300 V to mitigate the effect of δ-electrons, was placed between the target and STARS to attenuate damage to the detector caused by forward flying fission fragments. Fission fragments were detected in a 140 μm Micron S2 detector located 10 mm upstream from the target. The fission detector

covered an angle range of 106° to 131° relative to the beam axis. Each silicon detector had a 3000 angstrom gold backing for electrode contact and was segmented into the electrical equivalent of 24 rings on one side and 8 sectors on the other side. A target wheel was employed to switch between targets.

The ΔE, E and fission detectors were biased with 43 V, 200 V and 48 V, respectively. The signals were processed using 96 individual CHARGE8V Swan Research pre-amplifiers with gains of 47 mV/MeV for the ΔE and E detectors and 20 mV/MeV for the fission detector. These were connected to six 16-channel CAEN N568B shapers by 96 individual 10 m long RG-174 cables. The fast output from the shapers obtained leading edge discrimination by modified LeCroy 1806 discriminators. The discriminator thresholds were set at 60 mV, which corresponds to an energy threshold of approximately 800 keV. The master trigger pulse was considered valid when a single signal from the ΔE and E detectors were sensed within a 200 ns time window. The master trigger rate ranged between 4 and 8 kHz during the experiment. Once a valid signal occurred, the delayed shaped slow output of the shaper channels were digitized using SILENA 4418/V ADCs with a 4 μs time gate. The particle-fission timing was obtained using a time-to-amplitude converter module digitized by an Ortec AD413 peak-sensing ADC. Data were monitored online using the KMAX data acquisition system.

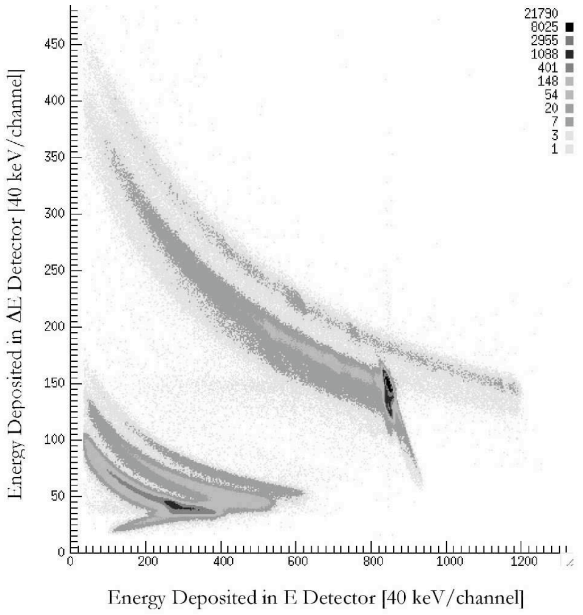

FIG. 2: Particle identification plot obtained from 42 MeV ^{3}He particles on ^{238}U for a given sector at an angle of 52 degrees with respect to the beam axis. The alpha particle "banana" appears at the top right of the figure and extends to higher energies than the ^{3}He curve, due to the positive Q-value for the reaction.

IV. DATA ANALYSIS AND RESULTS

By plotting energy loss (ΔE) versus residual energy (E), standard particle identification was accomplished for events in which a single interaction occurred in the telescope as shown in Figure 2. Event reconstruction was accomplished in the cases in which a particle traversed multiple rings when passing through a detector, leaving a fraction of its energy in each, or in the case of induced charge on adjacent electrodes. Using free form alpha particle gates, the total energy of the particle was reconstructed from the sum of the ΔE and E detector energies as well as calculations of energy losses in the target, aluminum shield and gold backing.

The total fission energy spectrum for ^{238}U(^{3}He,αf) is shown in Figure 3. In order to differentiate fission fragments from backscattered light-ion contaminants, a gate was made on the fission spectra for both targets. Fission fragments are distinguished from backscattered light-ion contaminants by an inflection point in the fission fragment energy spectrum. This is indicated in Figure 3 by the arrow pointing to the well centered around channel 300. Events to the right of this cutoff were taken as valid fission fragment events. The sensitivity of the extracted cross section to the position of the fission cutoff gate introduces an uncertainty in the measurement of ± 0.85%.

Only a fraction of the fission fragments are detected

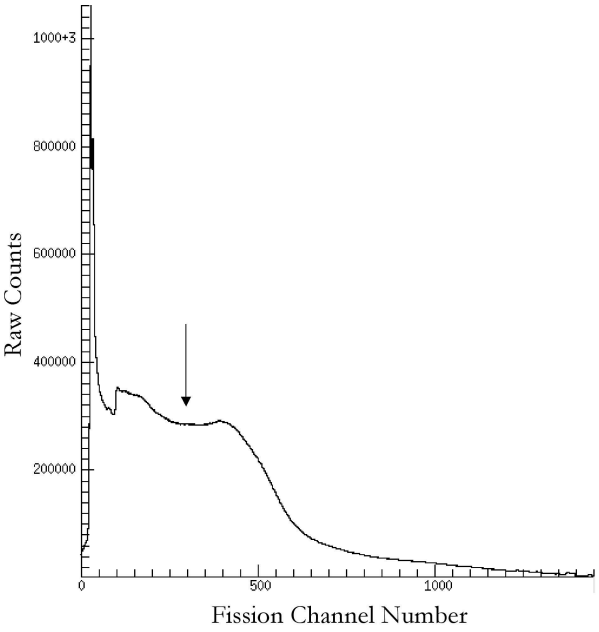

FIG. 3: Total fission energy spectrum for ^{238}U(^{3}He,αf) as a function of channel number. The arrow represents the fission cutoff energy. Events with energy greater than this cutoff were considered clean fission events.

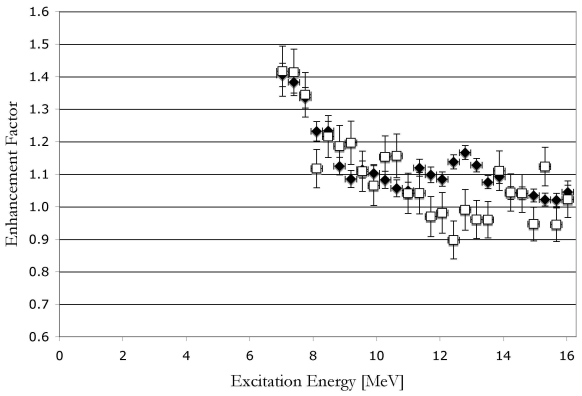

FIG. 4: Enhancement factor for fission fragment detection as a function of excitation energy for ^{238}U (filled diamonds) and ^{235}U (open squares). The x-error bars represent energy bin width. Note the zero-suppressed ordinate axis.

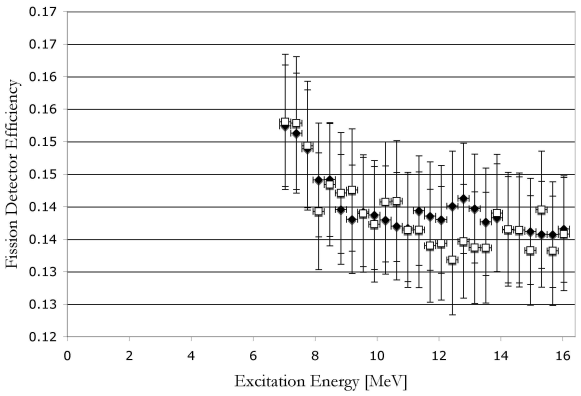

FIG. 5: Fission fragment detector efficiency as a function of excitation energy for ^{238}U (filled diamonds) and ^{235}U (open squares). The x-error bars represent energy bin width. Note the zero-suppressed ordinate axis.

in coincidence with the outgoing alpha particle. For isotropic emission, this fraction is the geometric efficiency of the fission detector, 0.14 ± 0.01. However, an enhancement in the fission detector efficiency could arise from a forward-peaked fission fragment angular distribution [15]. To determine if anisotropies existed in the fission fragment angular distributions, a fission fragment enhancement factor (EF) was extracted from the data. The EF is defined as the number of in-plane fission events relative to the number of out-of-plane events, normalized to unity using geometric factors. The EF was extracted as a function of excitation energy for fission events from ^{238}U and ^{235}U and is shown in Figure 4. The EF for both nuclei deviates from isotropy, as expected. The upward trend in the ^{238}U data from approximately 11 to 13 MeV and in the ^{235}U data from approximately 12 to 14 MeV arises from negotiation of the second chance fission barrier. This is manifest as an increase in the EF, because as the second chance fission channel opens, fission tends to proceed through the discrete states on top of the fission barrier.

The enhancement factors were used to generate energy-dependent fission detector efficiencies, given in Figure 5. For excitation energies greater than 13 MeV, there is no statistically significant enhancement in the geometrical efficiency due to fission fragment anisotropies. The fission detector efficiencies for the two nuclei are equal within experimental uncertainty and thus no correction is necessary in the ratio analysis.

For cross sections calculated using the SRM, a normalization factor relating the data for the two targets must be extracted, as shown in Equation 12. To deduce the number of uranium atoms in the target, a kinematically clean region from oxygen, nitrogen and carbon contamination was determined. The number of (^{3}He,α) events in this energy range are termed N_{clean}. The integrated beam current and acquisition system live time is assumed to be proportional to the total number of properly digitized master trigger events, N_{events}, scaled by the number of kinematically clean events. We assume that the number of reaction events is also proportional to the geometric cross section of the nucleus, which goes as $A^{2/3}$, where A is the mass number. The normalization factor for reactions on ^{238}U relative to ^{235}U is then given by

$$A_{norm} = \frac{^{238}N_{events}}{^{238}N_{clean}} \frac{^{235}N_{clean}}{^{235}N_{events}} \frac{^{235}\sigma_{geom}}{^{238}\sigma_{geom}} = 0.085 \pm 0.004 \quad (15)$$

A. ^{236}U(n,f) from an Absolute Surrogate Measurement

The absolute surrogate measurement is carried out as described by Equation 9. The alpha-fission coincidence spectrum for ^{238}U(^{3}He,αf) or numerator of Equation 9 was determined, as shown in the top panel of Figure 6. The alpha particle singles spectrum or denominator of Equation 9, as shown in the open squares in Figure 7, was extracted as a function of excitation energy in the compound nucleus. The alpha particle singles spectrum exhibited significant bleedthrough from ^{3}He elastic scattering, shown in Figure 7 as a peak at 14.2 MeV, as well as oxidative target contamination. The small hump centered at 13 MeV is due to (^{3}He,α) events on the ground state of ^{16}O. The total alpha particle singles spectrum used in the denominator of the absolute surrogate measurement was modified in the contaminant region with a linear interpolation, shown by the black line in Figure 7. The fission probability was corrected for the fission detector efficiency as a function of excitation energy, given in Figure 5. The fission probabilities were converted to a cross section by multiplying by the ^{236}U formation cross section obtained using a FLAP 2.2 optical model calculation [14].

The extracted cross section is shown in Figure 8. The

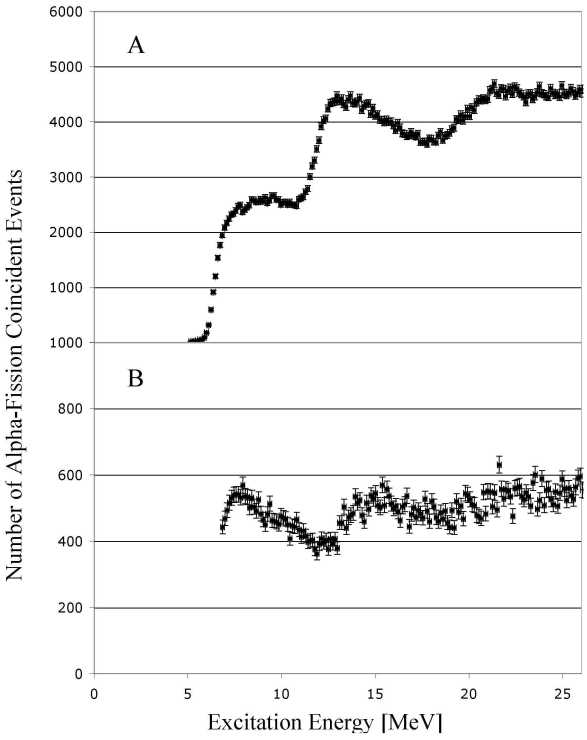

FIG. 6: Alpha fission coincidence spectra generated from A. ^{238}U(^{3}He,αf) and B. ^{235}U(^{3}He,αf) as a function of excitation energy. The coincidence spectra for each data set begins at the neutron separation energy for the appropriate compound nucleus.

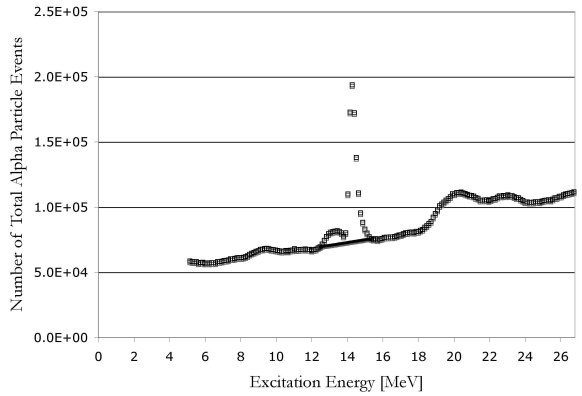

FIG. 7: The total number of alpha particle events from ^{238}U(^{3}He,α) as a function of equivalent neutron energy. The x- and y-error bars are smaller than the data points. The open squares represent the raw alpha particle singles spectrum. The alpha particle singles spectrum was modified, with linear smoothing across the contamination peaks, represented here by a line. The data begin at 5.13 MeV, the neutron separation energy for the ^{237}U compound nucleus.

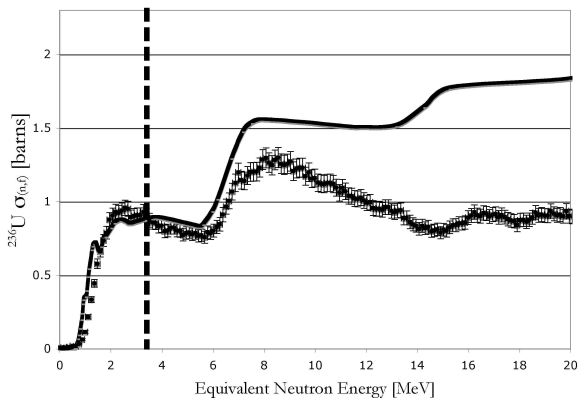

FIG. 8: ^{236}U(n,f) cross section obtained from an absolute surrogate measurement as a function of equivalent neutron energy. The black squares represent the experimental data and the solid line is the ENDF/B-VII library result. Data for equivalent neutron energies greater than the dashed vertical line are subject to contamination due to target impurities.

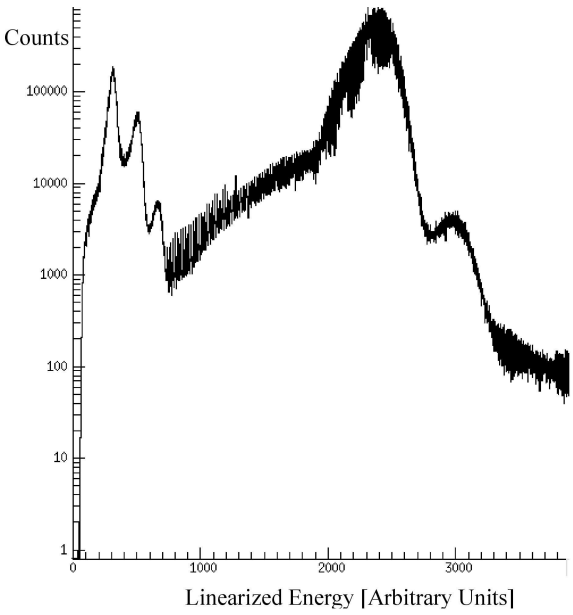

FIG. 9: A linearized particle identification spectrum for reaction products from ^{3}He on ^{238}U at an angle of 38° with respect to the beam axis and summed over all sectors. The peaks in the spectrum from left to right represent protons, deuterons, tritons, ^{3}He particles and alpha particles, respectively.

shape of the data trends well with the ENDF/B-VII results up to approximately 3.3 MeV, but the experimental data are lower in energy by as much as 50%. From 3.3 to 7.5 MeV, data are consistently lower in energy by 10% relative to the evaluated results. As the first-chance fission barrier is negotiated and up to ∼7.5 MeV, the experimental data appear to have the correct shape, but are offset relative to the evaluated data. Above 7.5 MeV, the data completely diverge from the evaluated result.

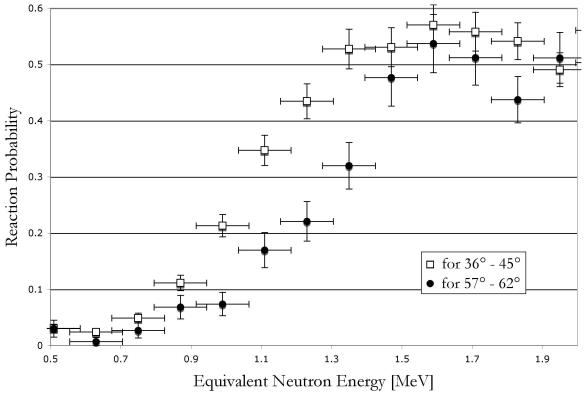

FIG. 10: The arbitrarily normalized absolute surrogate reaction probability for the ^{236}U(n,f) cross section as a function of angle. Data represented by open squares cover an angle range of 36° to 45° relative to the beam axis. Data represented by filled circles cover an angle range of 57° to 62° relative to the beam axis.

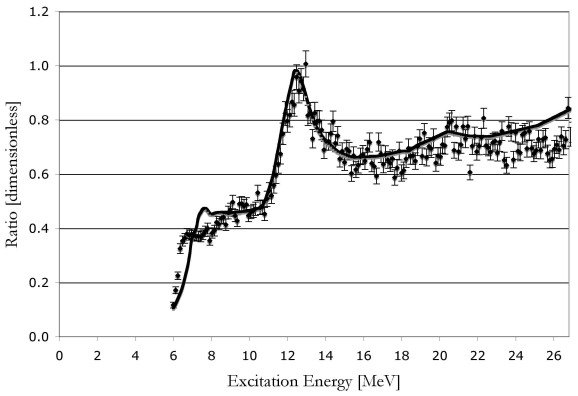

FIG. 11: The data points represent the normalized ratio of the ^{238}U(^{3}He,αf) to ^{235}U(^{3}He,αf) events as a function of excitation energy. The solid line is the ratio of the ^{236}U(n,f) to ^{233}U(n,f) cross sections calculated from the ENDF/B-VII library. The data begin at 6.84 MeV, the neutron separation energy for the ^{234}U compound nucleus.

This is the result of a very high ratio of ^{3}He to ^{4}He, illustrated in the linearized particle identification spectrum shown in Figure 9, and is manifest as ^{3}He bleedthrough into the alpha particle gate. This effect is exacerbated by oxidative and carbon contamination on the target, a known problem in absolute surrogate measurements [16], and resulted in a larger number of perceived (^{3}He,α) reactions on uranium, thus driving the fission probability down.

B. Absolute Surrogate Measurement as a Function of Angle

Given that the master trigger required a ΔE-E coincident event, the rings of the particle telescope covered an effective angle range of 36° to 62° relative to the beam axis and thus sampled different angular momentum distributions. An arbitrarily normalized absolute surrogate ^{236}U(n,f) reaction probability was extracted as a function of angle for two angle bins, 36° to 45° and 57° to 62° relative to the beam axis, as shown in Figure 10. There is a significant difference in the cross sections obtained for these two bins, with deviations as large as a factor of two in the energy range from 0.5 to 2 MeV, but the two measurements converge on either end of this energy range. This suggests that the Weisskopf-Ewing approximation is not valid in the energy range from 0.5 to 2 MeV. However, disparities are not as severe in the same energy range for the absolute surrogate cross section measurement, shown in Figure 8, as compared with the ENDF/B-VII results. This may be because the angular momentum population generated by the surrogate reaction averaged over all angles samples a similar angular momentum distribution at low energies as the neutron-induced reaction.

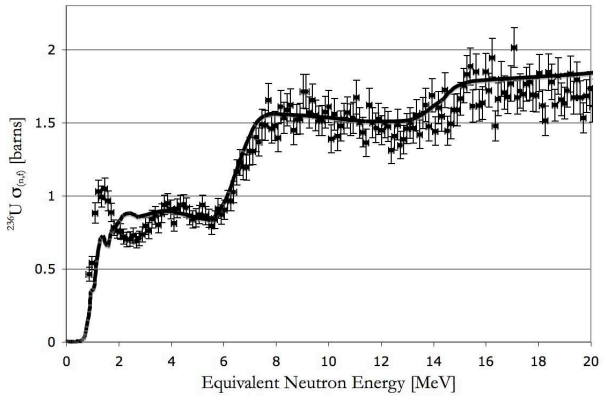

FIG. 12: The data points represent the ^{236}U(n,f) cross section determined using the SRM relative to the ^{233}U(n,f) cross section as a function of equivalent neutron energy. The solid line is the ENDF/V-BII library evaluation for this cross section.

C. ^{236}U(n,f) from the SRM

As described in Equation 14, the SRM required two alpha-fission coincidence measurements, illustrated in Figure 6. The ^{237}U* coincident data (top panel) exhibit a staircase pattern, typical for a nucleus for which the neutron binding energy is less than the fission barrier. For ^{234}U* (bottom panel), the neutron binding energy is greater than the fission barrier and thus, the number of alpha-fission coincidences increases with increasing energy until the nucleus has enough energy to emit a neutron. Then, fission and neutron emission are in competition until the nucleus has enough energy to emit two neutrons, and so on.

The normalized ratio as a function of excitation energy is shown in Figure 11. The data trend nicely with

the ENDF/B-VII results from 9 to 26.8 MeV. Discrepancies are present at excitation energies in the range of 6.8 – 9 MeV, with differences up to 40%. To obtain the ^{236}U(n,f) cross section shown in Figure 12, the ratio data were multiplied by the ENDF/B-VII ^{233}U(n,f) cross section matched at excitation energy and the result was shifted into equivalent neutron energy by subtracting the neutron separation energy of the ^{237}U compound nucleus from the excitation energy. The data trend nicely with the evaluated results except in the energy range of 1 – 3.5 MeV, where discrepancies on the order of 50% are present. At the onset of second chance fission at energies above 16 MeV, discrepancies exist in the data on the order of 10%, possibly due to the increasing pre-equilibrium component at this energy. Possible explanations for the significant deviation of the data in the energy range of 1 – 3.5 MeV include unjustified application of the Weisskopf-Ewing approximation, notable disparities in the spin and parity distributions of the two compound nuclei used in forming the ratio, or both. Deviations in the SRM-derived fission cross section and model predictions [7] are most pronounced at low excitation energies in the transition state nucleus, a region in which the Weisskopf-Ewing approximation may not be valid due to significant contributions from discrete states. However, the unusual behavior of the SRM cross section in this energy range is not well understood and further study is warranted.

V. CONCLUSIONS

We have measured the ^{236}U(n,f) cross section using both the absolute surrogate technique and the SRM. The results from the absolute surrogate measurement are applicable at equivalent neutron energies less than 3.3 MeV and above 3.3 MeV the data from the SRM are relevant. The shape of the ^{236}U(n,f) cross section derived using the absolute surrogate technique trends nicely with ENDF/V-BII below 3.3 MeV and is plagued by target contamination above this energy. This measurement exhibited an angular dependence in the energy range from 0.5 to 2 MeV, indicative of J^{π}-dependent branching ratios and thus, a deviation from the Weisskopf-Ewing limit. The SRM ^{236}U(n,f) cross section is consistent with ENDF/V-BII results from 3.5 to 20 MeV, but significant deviations are present in the data below 3.5 MeV. The discrepancy at low energy may indicate a breakdown of the Weisskopf-Ewing assumption, but these results require further study.

Acknowledgments

We wish to acknowledge the fruitful discussions and advice of S. Prussin and W. Younes. We would like to thank the 88–Inch Cyclotron operations and facilities staff for their help in performing this experiment. This work was performed under the auspices of the U.S. Department of Energy by the University of California, Lawrence Livermore National Laboratory under contract No. W-7405-Eng-48, Lawrence Berkeley National Laboratory under contract No. DE-AC03-76SF0098 and the University of Richmond and Yale University and under grant numbers DE-FG-05NA-25929, DE-FG02-05ER-41379 and DE-FG02-91ER-40609.

[1] J.D. Cramer and H.C. Britt, Nucl. Sci. Eng. **41**, 177 (1970).
[2] H.C. Britt and J.B. Wilhelmy, Nucl. Sci. Eng. **72**, 222 (1979).
[3] C. Plettner, H. Ai, C.W. Beausang, L.A. Bernstein, L. Ahle, H. Amro, M. Babilon, J.T. Burke, J.A. Caggiano, R.F. Casten, *et al.*, Phys. Rev. C **71**, 051602(R) (2005).
[4] W. Younes and H.C. Britt, Phys. Rev. C **67**, 024610 (2003).
[5] I. Thompson and J.E. Escher, Technical Report No. UCRL-TR-225984, Lawrence Livermore National Laboratory, Livermore, CA, 2006 (unpublished).
[6] W. Younes, private communication.
[7] J.E. Escher and F.S. Dietrich, Phys. Rev. C **74**, 054601 (2006).
[8] J.T. Burke, L.A. Bernstein, J. Escher, L. Ahle, J.A. Church, F.S. Dietrich, K.J. Moody, E.B. Norman, L. Phair, P. Fallon, *et al.*, Phys. Rev. C **73**, 054604 (2006).
[9] C.W. Beausang, S.R. Lesher, J.T. Burke, L.A. Bernstein, L. Phair, H. Ai, G. Gurdal,, L. Ahle, D.S. Brenner, M. Carpenter, *et al.*, Acta Phys. Pol., B. (to be published)
[10] S.R. Lesher, L.A. Bernstein, J.T. Burke, L. Phair, C.W. Beausang, H. Ai, D. Bleuel, R.M. Clark, P. Fallon, J. Gibelin, *et al.*, (unpublished).
[11] W. Hauser and H. Feshbach, Phys. Rev. **87**, 366 (1952).
[12] F.S. Dietrich, Technical Report No. UCRL-TR-201718, Lawrence Livermore National Laboratory, Livermore, CA, 2004 (unpublished).
[13] M.B. Chadwick, P. Oblozinsky, M. Herman, N.M. Greene, R.D. McKnight, D.L. Smith, P.G. Young, R.E. MacFarlane, G.M. Hale, S.C. Frankle, *et al.*, "ENDF/B-VII.0: Next Generation Evaluated Nuclear Data Library for Nuclear Science and Technology," *Nuclear Data Sheets*, **107**, pp. 2931-3060, 2006.
[14] F. S. Dietrich, private communication.
[15] R. Vandenbosch and J.R. Huizenga. *Nuclear Fission.* (Academic Press, New York, 1973), Ch. XIV.
[16] M. Petit, M. Aiche, G. Barreau, S. Boyer, N. Carjan, S. Czajkowski, D. Dassié, C. Grosjean, A. Guiral, B. Hass, *et al.*, Nucl. Phys. A **735**, 345 (2004).